Article

Remote Sensing and Mapping of Tamarisk along the Colorado River, USA: A Comparative Use of Summer-Acquired Hyperion, Thematic Mapper and QuickBird Data

Gregory A. Carter [1,2,*], Kelly L. Lucas [1], Gabriel A. Blossom [1], Cheryl L. Lassitter [3], Dan M. Holiday [1,3], David S. Mooneyhan [1], Danielle R. Fastring [4], Tracy R. Holcombe [5] and Jerry A. Griffith [2]

[1] Gulf Coast Geospatial Center, University of Southern Mississippi, Gulfport, Mississippi, 39501, USA; E-Mails: kelly.lucas@gcgcusm.org (K.L.L.); gblossom2020@yahoo.com (G.A.B.); dan.holiday@usm.edu (D.M.H.); david.mooneyhan@gcgcusm.org (D.S.M.)

[2] Dept. of Geography and Geology, University of Southern Mississippi, Hattiesburg, Mississippi, 39406, USA; E-Mail: griffith@usm.edu (J.A.G.)

[3] Dept. of Coastal Sciences, University of Southern Mississippi, Ocean Springs, Mississippi, 39564, USA; E-Mail: cheryl.lassitter@noaa.gov (C.L.L.)

[4] Dept. of Community Health Sciences, University of Southern Mississippi, Hattiesburg, Mississippi, 39406, USA; E-Mail: danielle.fastring@gmail.com (D.R.F.)

[5] Fort Collins Science Center, United States Geological Survey, Fort Collins, Colorado, 80526, USA; E-Mail: holcombet@usgs.gov (T.R.H.)

* Author to whom correspondence should be addressed; E-Mail: greg.carter@gcgcusm.org; Tel.: +1-228-276-1722; Fax: +1-228-276-1721

Abstract: Tamarisk (*Tamarix spp.*, saltcedar) is a well-known invasive phreatophyte introduced from Asia to North America in the 1800s. This report compares the efficacy of Landsat 5 Thematic Mapper (TM5), QuickBird (QB) and EO-1 Hyperion data in discriminating tamarisk populations near De Beque, Colorado, USA. As a result of highly correlated reflectance among the spectral bands provided by each sensor, relatively standard image analysis methods were employed. Multispectral data at high spatial resolution (QB, 2.5 m Ground Spatial Distance or GSD) proved more effective in tamarisk delineation than either multispectral (TM5) or hyperspectral (Hyperion) data at moderate spatial resolution (30 m GSD).

1. Introduction

The spread of invasive plant species to native ecosystems is a frequent consequence of land conversion, habitat fragmentation and commerce, resulting in diminished global biodiversity and ecosystem integrity [1,2]. Tamarisk (*Tamarix spp.* or saltcedar) is a well-known invasive phreatophyte introduced from Asia to North America in the 1800s as an ornamental or shade plant used subsequently for erosion control [3]. In the western USA, it occupies over 600,000 ha of riparian habitat [4] and continues to spread in semi-arid regions, consuming valuable resources [5–7]. Western states heavily infested with tamarisk include Texas, New Mexico, Colorado and California, where dense stands impact native vegetation and cause extensive groundwater loss [8]. Along the Colorado River, tamarisk has replaced much of the native riparian vegetation and reduced stream flow via sediment entrapment and groundwater depletion [7]. Such water depletion and obstruction to flow may elevate soil salinity [9]. The cumulative effects of tamarisk invasions justify its ranking as one of the ten worst noxious weeds in the USA [10]. In order to facilitate the monitoring of tamarisk invasions and quantify the effectiveness of tamarisk management practices, there is a clear need for accurate and economical methods of detecting and mapping tamarisk.

Specific remote sensors and analytical methods used in tracking invasive species vary widely, depending on the geographical scale of interest. At a continental scale, relatively coarse spatial resolution (250 m Ground Spatial Distance or GSD) MODIS data have been used in mapping potential tamarisk habitat for the conterminous USA [11]. Although this approach would not have been suitable for the direct detection of tamarisk populations because of the coarse spatial resolution, the resulting map of current and potential tamarisk habitat is highly useful in predicting the spread of tamarisk. At intermediate spatial scales, multispectral imagery acquired by the Landsat Thematic Mapper (TM) (30 m GSD) were used to directly detect and classify tamarisk populations at the mouth of the Yellow River in China [12]. More recently, the use of Landsat 5 TM (TM5) data acquired during winter, when tamarisk branches were leafless, provided 98% discrimination of tamarisk from other riparian vegetation along the Arkansas River, Colorado, USA [13].

As with spatial resolution, enhanced spectral and radiometric resolutions may also be an advantage in the detection and mapping of invasive plants [2,14]. Tamarisk mapping accuracy reached 89% when a Mixture Tuned Matched Filtering algorithm was applied to airborne hyperspectral data acquired at 2.5 m GSD in Colorado [15]. In determining the effectiveness of biological control of tamarisk in several western USA states from airborne hyperspectral imagery acquired at 1–2 m GSD during early July and late August, near-infrared (768 or 777 nm), green (539 or 548 nm) and red (653 or 670 nm) spectral bands were most useful [8]. Similarly, the selection via hierarchical clustering of 569 nm, 702 nm, 719 nm and 770 nm spectral bands from airborne hyperspectral imagery acquired at 0.5 m GSD yielded optimal detection of tamarisk in Southern California [16]. Acquired from earth orbit at 30 m GSD, data from NASA's EO-1 Hyperion [17] were used to classify tamarisk in Western Nevada, USA [18]. When Discriminate Function Analysis was applied to the Hyperion data, tamarisk could be

mapped with greater accuracy compared with the use of Landsat Enhanced Thematic Mapper (ETM) data (86% versus 78%, respectively).

With respect to the use of data from orbital sensors, the preceding review indicates that the discrimination of tamarisk from other riparian vegetation is most accurate when tamarisk is leafless and data are acquired during winter [13]. However, we were interested in comparing the efficacy for tamarisk delineation among high-spatial-resolution, multispectral satellite imagery (2.5 m QuickBird) and 30 m hyperspectral (Hyperion) or multispectral (TM5) data. This required the use of spatially-overlapping, summer 2004 coverage from these sensors that were approximately coincident with a 2003–2004 field sampling of the study area, located along the Colorado River, Colorado, USA.

2. Methods

2.1. Study Area

The study area was located along the Colorado River near De Beque, Colorado (39º33' N, -108º2' W). Average elevation of the area is approximately 1,500 m, with the southeastern edge of the Roan Cliffs located to the northeast. The area contains substantial amounts of tamarisk that have been well-documented by a number of field survey teams. Tamarisk stands used in image classifications were located via GPS between January, 2003 and May, 2004. A total of 40 plots located within the De Beque 7.5 minute USGS quadrangle were surveyed using a purposive sample design [19] and relevé principles [20] to maximize variation in habitat. Plots were placed in each major vegetation zone to cover the full range of environmental gradients present. The relevé method quickly determines relative cover by species in a plot that represents a particular vegetation type.

The primary sampling unit was a 30 m × 30 m cluster plot which corresponded with the 30 m GSD of Hyperion and TM5 data. Within each of these 900 m^2 areas, nine subplots, each 10 m × 10 m (100 m^2) in dimension, allowed for analysis at the finer resolution enabled by QB data (2.5 m GSD). Within each of these plots and subplots, percent cover of tamarisk and other dominant vegetation was recorded.

2.2. Remote Sensing

TM5 and Hyperion data (USGS EROS Data Center, Sioux Falls, South Dakota, USA) acquired on July 13 and July 5, 2004, respectively, and QB data (Digital Globe, Longmont, Colorado, USA) acquired on August 16, 2004, corresponded with the approximate time of field sampling. Additionally, QB data acquired on June 8, 2005 were available for comparison with the 2004 QB data. Airborne hyperspectral data from the HyMap sensor (HyVista Corp., New South Wales, Australia) acquired on July 6, 2002, were used in calibrating the TM5 and QB data to reflectance units. While the dates of field sampling and image acquisition may differ, tamarisk populations in the study area are notably stable from year-to-year (T. Stohlgren, USGS, Fort Collins, CO, USA, personal communication). Thus, the surveyed locations of tamarisk stands were applicable for all image acquisitions.

2.3. Georectification and Reflectance Calibration

All images were registered using the nearest-neighbor resampling method to a rectified 1 m digital ortho quarter quad (DOQQ) of the De Beque area. Rectification of the Level I Hyperion and TM5 imagery was refined further to a root mean square error (RMSE) of less than 0.5 pixels. Rectification of QB standard-bundle imagery was refined to a RMSE of 0.4 and 0.5 pixels for the 2004 and 2005 acquisitions, respectively.

The HyMap imagery consisted of 126 spectral channels (bands) covering a 440 nm to 2,500 nm spectral range at a full-width-at-half-maximum (FWHM) bandwidth of approximately 15 nm. The flight altitude of 3,500 m produced a GSD of 3.7 m. The data were calibrated at-sensor to radiance units ($\mu W/cm^2$ nm sr) and processed subsequently to apparent reflectance using Fast Line-of-Sight Atmospheric Analysis of Hypercubes (FLAASH) (ENVI v. 4.2, ITT Visual Information Systems, Boulder, CO, USA). FLAASH employs an atmospheric correction based on MODTRAN 4+ radiative transfer models and corrects for absorptions by atmospheric water vapor, methane, oxygen, carbon dioxide and ozone on a pixel-by-pixel basis. The FLAASH calibration to apparent reflectance was refined using an Empirical Line calibration (ENVI v. 4.2) based on the in situ reflectance of an asphalt road collected in June, 2005 (ASD FS, Analytical Spectral Devices, Boulder, CO, USA). Although field measurements of asphalt road reflectance were not made simultaneously with image acquisitions, all data were acquired when the road surface was dry. Thus, the road was acceptable as a pseudo-invariant calibration target. The Empirical Line calibration forces spectral data to match field reference data using a linear regression for each band. When only one ground target is used, as in the present case, the regression line is assumed to pass through a zero origin. HyMap bands 1 (437 nm), 31 (873 nm), 63–66 (1,405–1,447 nm), 94 (1,805 nm), 95 (1,949 nm) and 126 (2,484 nm) were deleted due to strong atmospheric interference, detector overlap or detector insensitivity. The remaining 117 bands spanned the 443 nm to 2,468 nm range.

Next, regions-of-interest (ROI) representing specific pseudo-invariant targets of lake water and bare gravel were created using the HyMap data. ROI spectra of these surfaces were extracted to a spectral library (ENVI v. 4.2). The water served as a low-reflectance target while reflectance of the bare gravel was substantially greater. HyMap spectral reflectances of these dark-to-bright targets were re-sampled to TM5 or QB spectral bands (ENVI v. 4.2) and used in an Empirical Line calibration of the TM5 and QB data. This corrected the data for atmospheric interference and yielded units of percentage reflectance. QB data were acquired in four broad spectral bands centered at 485, 560, 660 and 830 nm (Table 1) at 2.5 m GSD and 11-bit radiometric resolution. TM5 data included these bands as well as mid-infrared bands at 1,650 and 2,215 nm (Table 1) and were acquired at 30 m GSD with 8-bit radiometric resolution.

Hyperion data include 242 spectral bands ranging from 356 nm to 2,577 nm at a FWHM bandwidth of 10 nm and 12-bit radiometric resolution. Because Hyperion bandwidths are narrower than the ca. 15 nm bandwidths in HyMap data, the latter could not be used to calibrate the Hyperion data to reflectance units. Instead, Hyperion data were spectrally subset to remove bands 1–8 (357–417 nm) and 225-242 (2,406–2,577 nm), owing to data noise, and bands 58–70 (925–1,068 nm) and 71–77 (852–912 nm) were eliminated due to detector overlap. The remaining 196 Hyperion bands covered the 426 nm to 2,396 nm spectral range and were calibrated to apparent reflectance using

FLAASH. The field spectroradiometric data could not be used to refine the Hyperion calibration because the gravel road was not clearly visible in the 30 m GSD Hyperion image. Inspection of the reflectance-calibrated Hyperion data revealed substantial noise or extreme image striping in the 1,356–1,457 nm, 1,820–1,992 nm, 2,022–2,042 nm, 2,062–2,082 nm and 2,284–2,396 nm regions. These spectral regions were deleted, leaving 148 bands for potential use in tamarisk mapping.

2.4. Image Classification

Initially, an unsupervised classification algorithm (isodata, ENVI v. 4.2) was applied to the TM5, QB and Hyperion data. This allowed a preliminary assessment of tamarisk discrimination in the De Beque area. Additionally, principal components analysis (PCA) [21,22] and the Minimum Noise Fraction (MNF) procedure [21] were applied to the Hyperion data (ENVI v. 4.2). However, band correlation analysis (ENVI v. 4.2) applied to each reflectance-calibrated data set indicated substantial redundancy among spectral bands in the reflectance of vegetated terrain (see Results). Based on these initial assessments, data dimensionality was reduced by removing redundant bands. This facilitated use of the Maximum Likelihood (ML) algorithm and normalized-difference indices [21,22] in subsequent comparisons among sensor data in tamarisk delineation. ML was selected because it is widely accepted and generally provides the greatest accuracy among various supervised classification procedures [21]. It computes the probability that a certain pixel belongs to one of a pre-defined number of classes, taking into account the variability in each ROI and assuming that training data statistics in each band for each class are normally distributed. The pixel is then assigned to the class to which it most likely belongs. Inspection of training data for the bands selected from each sensor indicated general normality with slight skewing in some bands, but no bi-modal distributions. Nevertheless, as a parametric method, ML is robust to violations of training-data normality and performs well when training data are limited [23].

Training data for supervised classifications of TM5 or Hyperion images were based on 30 m plots which contained 80% or greater coverage by tamarisk. For QB classifications, 10 m subplots containing 100% tamarisk cover were used. The same 30 m plots and 10 m subplots were used in determining value ranges of remote sensing indices that were representative of tamarisk stands. Indices applied were the NDVI [23] and a similar index which incorporated green-band rather than red-band reflectance (Green NDVI or GNDVI). Additionally, data from these plots and subplots were used to assess image classification accuracy. For data from each sensor, 40% of plot data were used in classification training. The remaining 60% were reserved for post-classification accuracy assessment. All image classifications were based on sample plot (training) areas of at least 0.3 ha.

Classification accuracy was determined by error matrix and the K_{hat} coefficient of agreement [21,22]. This produced values for errors of omission (percentage of tamarisk pixels that were not classed as tamarisk) and errors of commission (percentage of non-tamarisk pixels that were classed as tamarisk). K_{hat} represents the extent to which a given classification procedure improved classification accuracy relative to a random classifier [22]. Thus, for example, $K_{hat} = 0.33$ would indicate a 33% improvement in accuracy relative to classification by chance.

3. Results

Initial assessments of the TM5, QB and Hyperion data indicated that an unsupervised classification approach was inadequate for tamarisk detection. Because Hyperion bands within a given spectral region tended to be strongly correlated for vegetated riparian and agricultural areas, the data set was reduced, with no significant loss of information, to include only those spectral bands which approximated the central wavelengths of the TM5 bands (Figure 1, Table 1). In total, the resulting 6-band set correlated with the original Hyperion spectrum at $r \geq 0.95$ (Table 2) and yet included band pairs with $r \geq 0.72$ which were potentially useful in tamarisk delineation (Table 3). The use of Hyperion PCA or MNF bands versus the minimally-correlated band set yielded no improvement in ML classification accuracy.

Figure 1. Spectral correlations (*r*) of Hyperion reflectance with reflectance in bands of central wavelength similar to TM5 bands 1-5 and 7. Dark triangles are located at the reference central wavelength (listed in each graph) where *r* = 1.
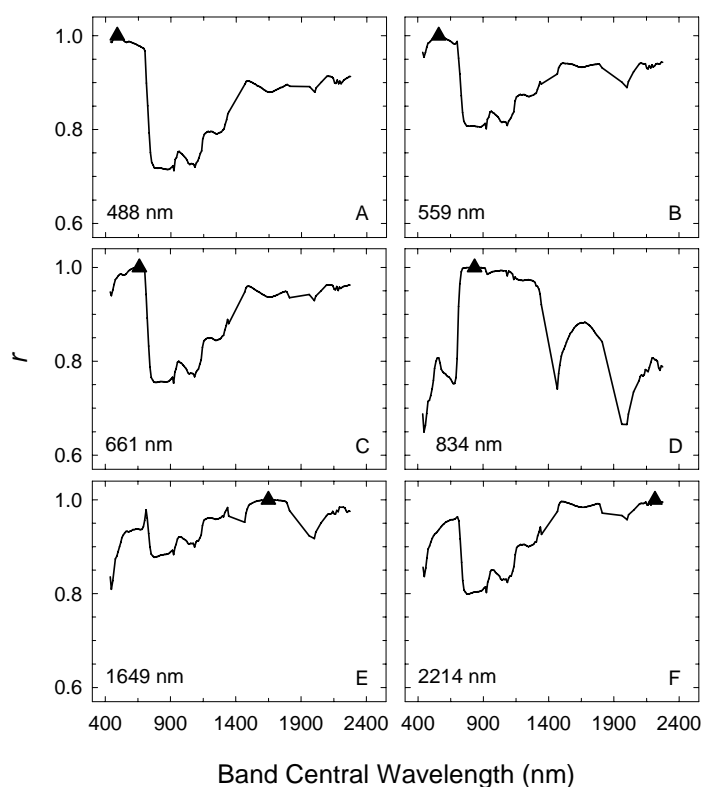
In addition to correlations among Hyperion bands, redundancy was found also among TM5 and QB bands (Table 3). For all three sensors, reflectance in the blue band correlated strongly with other visible-spectrum bands. Thus, and owing to greater blue-band susceptibility to atmospheric interference, the blue band was eliminated from each data set prior to image classifications. Likewise, green versus red bands correlated strongly (Table 3). Consequently, the red band was not included in multiband ML analyses but was used necessarily in classifications based on the NDVI [24]. As a result of these band correlations (Table 3), image classification procedures utilized a maximum of four TM5

or Hyperion bands, or two QB bands. ML classifications incorporated green, near-infrared and two mid-infrared bands from TM5 or Hyperion, or the green and near-infrared QB bands (Table 1).

Table 1. Central wavelength and approximate bandwidth of QB, TM5 and Hyperion bands used in tamarisk delineation.

QB or TM5			Hyperion		
Band	**Wavelength (nm)**	**Bandwidth (nm)**	**Band**	**Wavelength (nm)**	**Bandwidth (nm)**
1	485	70	14	488	10
2	560	80	21	559	10
3	660	60	31	661	10
4	830	140	48	834	10
TM5					
5	1,650	200	150	1,649	10
7	2,215	270	206	2,214	10

Table 2. Ranges in band central wavelength through which Hyperion reflectance data correlated at $r \geq 0.95$ with reflectance at central wavelengths similar to TM5 bands (given in parentheses).

Hyperion Band	Central Wavelength (nm)	Correlated Wavelength Range (nm)
14 (1)	488	437–702
21 (2)	559	437–712
31 (3)	661	457–702
		1,477–1,558
		2,052–2,274
48 (4)	834	722–1,326
150 (5)	1,649	701–722
		1,155–1,810
		2,052–2,274
206 (7)	2,214	610–722
		1,467–2,274

Maximum classification accuracies, determined by K_{hat}, were produced by NDVI threshold values from 2004 Hyperion and QB data, whereas a four-band ML classification produced maximum accuracy from 2004 TM5 data (Table 4). Generally, K_{hat} values of 0.4 to 0.8, as with Hyperion and QB results, indicate moderate to good improvement in classification accuracy relative to a random classification [22,25]. QB 2004 data yielded the greatest classification accuracy, followed by Hyperion and TM5. Results from 2005 QB data were similar to those from 2004 data, except the GNDVI yielded a greater accuracy than the NDVI. The greatest accuracy produced in classifications of TM5 data indicated little improvement over a random classification ($K_{hat} = 0.18$).

In the use of 2004 Hyperion, TM5 and QB data for tamarisk mapping, 88%, 80% and 91% of reference pixels, respectively, were classified correctly (Table 5). However, errors of commission, the inclusion of non-tamarisk pixels as tamarisk pixels, were high for all classifications (Table 5). In particular, errors of commission were demonstrated in best-classification images for each sensor by the inclusion of agricultural fields as well as riparian habitat in the tamarisk class (Figure 2). Errors of omission, the failure to include known tamarisk areas in the tamarisk class, were also appreciable except for the Hyperion classification (Table 5). Classification of 2005 QB data produced results similar to the classification of 2004 QB data. Thus, a 2005 QB classified image and corresponding percentage accuracies are not shown.

Table 3. Matrices of correlation among TM5, QB and selected Hyperion bands for vegetation in the De Beque, CO area.

| Band	Correlation Coefficient (r)				
	TM5 or QB Band				
	1	2	3	4	5
TM5					
2	0.95				
3	0.94	0.94			
4	-0.14	-0.09	-0.14		
5	0.74	0.79	0.81	0.13	
7	0.85	0.86	0.89	-0.13	0.92
QB					
2	0.98				
3	0.96	0.98			
4	-0.05	0.01	-0.05		
	Hyperion Band				
	14	21	31	48	150
Hyperion					
21	0.99				
31	0.98	0.99			
48	0.72	0.81	0.76		
150	0.88	0.93	0.94	0.88	
206	0.90	0.94	0.96	0.80	0.98

Table 4. Accuracies of Tamarisk mapping (K_{hat}) in classifications derived from Hyperion, TM5 and QB data.

Algorithm	K_{hat}			
	Hyperion, 2004	TM5, 2004	QB, 2004	QB, 2005
ML, 4-band	0.18	0.18	-	-
ML, 2-band	0.23	0.10	0.69	0.66
GNDVI	0.36	0.00	0.73	0.72
NDVI	0.50	-0.03	0.74	0.64

Table 5. Algorithms that yielded maximum accuracies in tamarisk classification when applied to 2004 Hyperion, TM5 and QB data.

Sensor	Algorithm	%		
		Accuracy	**Omission Error**	**Commission Error**
Hyperion	NDVI	88	0	62
TM5	ML, 4-band	80	40	83
QB	NDVI	91	18	78

Figure 2. Generalized map (a) with tamarisk distributions (red) estimated for the De Beque, Colorado area based on classifications of Hyperion (b), TM5 (c) and QB (d) data. These images represent the greatest classification accuracy for each sensor and were produced from ML classification of TM5 bands 2, 4, 5 and 7 (c) or NDVI thresholds for Hyperion (b) and QB (d).
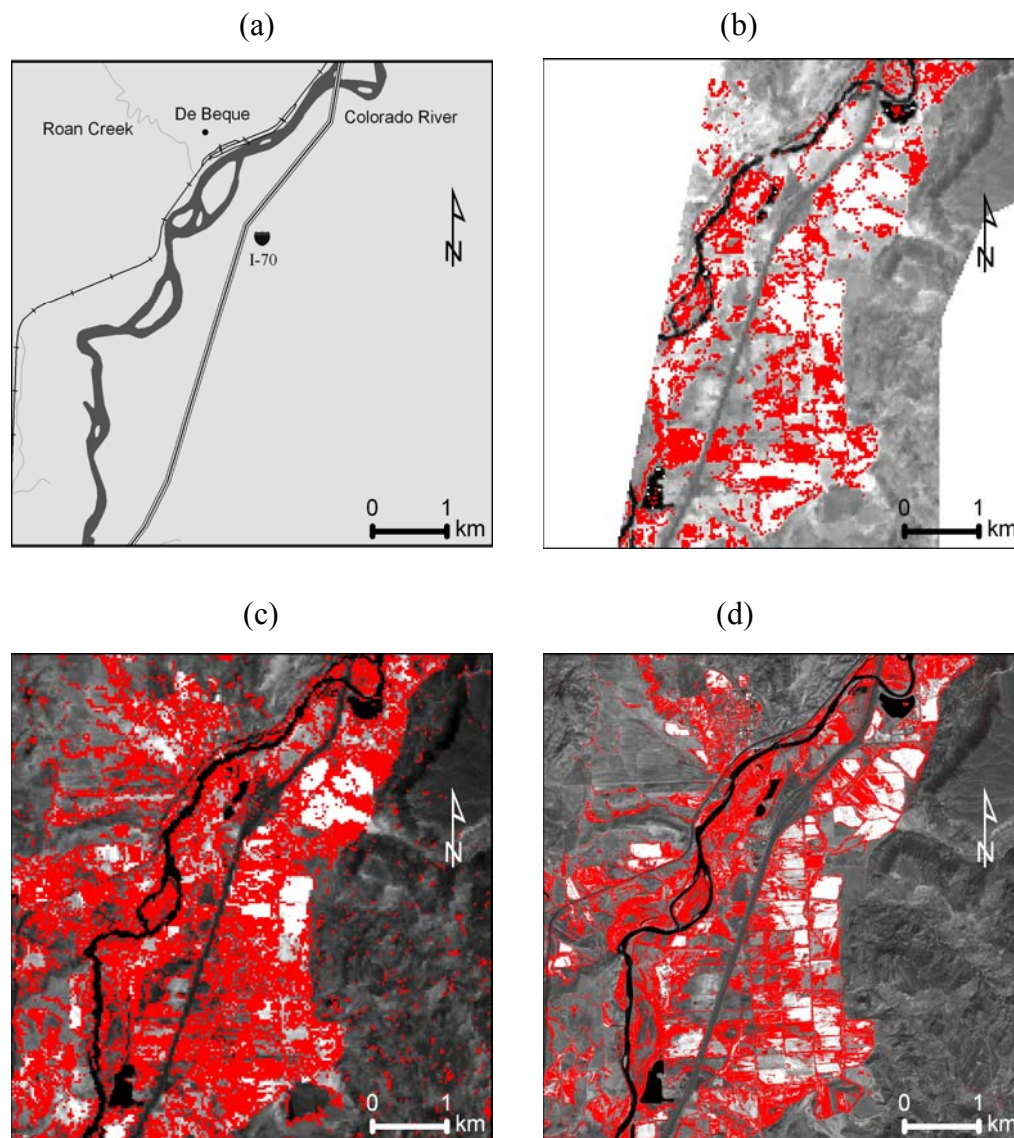
4. Discussion and Conclusions

High-spatial-resolution measurements of green or red along with near-infrared reflectance yielded substantial improvement in K_{hat}, similar to the results of earlier studies which relied on airborne hyperspectral data [8,16]. Multispectral data at a 2.5 m GSD (QB) proved more effective in tamarisk mapping than either the same bands (TM5) or hyperspectral data (Hyperion) at 30 m GSD. The high spectral resolution of Hyperion did not yield an improvement over QB classifications, even though the radiometric precision of Hyperion (12-bit) is twice that of QB (11-bit). Similar spectral characteristics among riparian species during summer [13] and within-pixel spectral mixing reduced the utility of high spectral resolution. Also, there were few ground plots containing 80–100% tamarisk coverage that were of sufficient size to yield 30 m GSD reference pixels. In contrast, the combination of high spectral and spatial resolutions previously enabled high-accuracy mapping of tamarisk in the De Beque area [15] and in Southern California [16] and has been useful in monitoring the biological control of tamarisk in Nevada [8].

At comparable GSD, the greater spectral and radiometric resolutions of Hyperion versus TM5 (8-bit) data enhanced tamarisk delineation. Similarly, in western Nevada, Hyperion yielded greater tamarisk classification accuracies than ETM+ [18].

For QB data, overall classification accuracy ranged to 91% but errors of commission were large. This likely was a consequence of data being acquired in summer when the foliage of riparian plant species was green [13]. The moderate spectral resolution of QB was not sufficient to distinguish subtle spectral differences among vegetation types. Thus, non-tamarisk riparian vegetation and portions of agricultural fields were frequently included in the tamarisk class. Had the imagery been acquired during autumn, when the color of tamarisk foliage changes to yellow-orange [9], or during late-autumn to winter when tamarisk is leafless [13], errors of commission likely would have been reduced.

Acknowledgements

References and Notes

1. Sanders, N.J.; Gotelli, N.J.; Heller, N.E.; Gordon, D.M. Community disassembly by an invasive species. *Proc. Natl. Acad. Sci.USA* **2003**, *100*, 2474–2477.
2. Underwood, E.C.; Ustin, S.L.; DiPietro, D. Mapping nonnative plants using hyperspectral imagery. *Remote Sens. Environ.* **2003**, *86*, 150–161.
3. Pearce, C.M.; Smith, D.G. Saltcedar: distribution, abundance, and dispersal mechanisms, northern Montana, USA. *Wetlands* **2003**, *23*, 215–228.
4. Lovich, J.E. A brief review on the impacts of Tamarisk or Saltcedar on biodiversity in the New World. In *Saltcedar Management and Riparian Restoration Workshop*, Las Vegas, NV, USA, 1996.

5. Robinson, T.W. Introduction, spread and areal extent of Saltcedar (*Tamarix*) in the western states. *USGS Professional Paper* **1965**, 491-A:1–491-A:12.

6. Everitt, B.L. Ecology of saltcedar—a plea for research. *Environ. Geol.* **1980**, *3*, 77–84.

7. Sala, A.; Smith, S.D.; Devitt, D.A. Water use by *Tamarix ramosissima* and associated phreatophytes in a Mojave Dessert floodplain. *Ecol. Appl.* **1996**, *6*, 888–898.

8. Anderson, G.L.; Carruthers, R.I.; Shaokui, G.E.; Gong, P. Monitoring of invasive *Tamarix* distribution and effects of biological control with airborne hyperspectral remote sensing. *Int. J. Remote Sens.* **2005**, *26*, 2487–2489.

9. Everitt, J.H.; Escobar, D.E.; Alaniz, M.A.; Davis, M.R.; Richerson, J.V. Using spatial information technologies to map Chinese Tamarisk (*Tamarix chinensis*) infestations. *Weed Sci.* **1996**, *44*, 194–201.

10. Lesica, P.; Miles, S. Ecological strategies for managing Tamarisk on the C. M. Russell National Wildlife Refuge, Montana, USA. *Biol. Conserv.* **2004**, *119*, 535–543.

11. Morisette, J.T.; Jarnevich, C.S.; Ullah, A.; Cai, W.; Pedelty, J.E.; Gentle, J.E.; Stohlgren, T.J.; Schnase, J.L. A tamarisk habitat suitability map for the continental United States. *Front. Ecol. Environ.* **2006**, *4*, 11–17.

12. Fang, H.; Xu, J. Land cover and vegetation change in the Yellow River Delta Nature Reserve analyzed with Landsat Thematic Mapper data. *Geocarto Int.* **2000**, *15*, 1–7.

13. Groeneveld, D.P.; Watson, R.P. Near-infrared discrimination of leafless saltcedar in wintertime Landsat TM. *Int. J. Remote Sens.* **2008,** *29*, 3577–3588.

14. Glenn, N.F.; Mundt, J.T.; Weber, K.T.; Prather, T.S.; Lass, L.W.; Pettingill, J. Hyperspectral data processing for repeat detection of small infestations of leafy spurge. *Remote Sens. Environ.* **2005**, *95*, 399–412.

15. Laes, D.; Maus, P.; Fisk, H.; Davern, T. Tamarisk remote sensing inventory and assessment. In *Progress Report to the Remote Sensing Steering Committee*. USDA Forest Service Engineering, Remote Sensing Applications Center: Salt Lake City, UT, USA, 2003; pp. 1–16.

16. Hamada, Y.; Stow, D.A.; Coulter, L.L.; Jafolla, J.C.; Hendricks, L. W. Detecting Tamarisk species (*Tamarix* spp.) in riparian habitats of Southern California using high spatial resolution hyperspectral imagery. *Remote Sens. Environ.* **2007**, 109, 237–248.

17. Pearlman, J.S.; Barry, P.S.; Segal, C.C.; Shepanski, J.; Beiso, D.; Carman, S.L. Hyperion, a space-based imaging spectrometer. *IEEE T. Geosci. Remote* **2003**, *41*, 1160–1173.

18. McGwire, K.M.; Schulz, B. Hyperspectral monitoring of invasive, non-native plant species with EO-1 Hyperion imagery. In *Final Report, NASA EO-1 Science Team Grant NASA-NCC5-486*, Goddard Space Flight Center: Greenbelt, MD, USA, 2002.

19. Guarte, J.M.; Barrios, E.B. Estimation under purposive sampling. *Commun. Stat.: Simul. C.* **2006**, *35*, 277–284.

20. Mueller-Dombois, D.; Ellenberg, H. *Aims and Methods of Vegetation Ecology*, John Wiley & Sons: New York, NY, USA, 1974.

21. Jensen, J.R. *Introductory Digital Image Processing: A Remote Sensing Perspective*, Prentice-Hall: Upper Saddle River, NJ, USA, 2005.

22. Lillesand, T.M.; Kiefer, R.W.; Chipman, J.W. *Remote Sensing and Image Interpretation*, John Wiley & Sons: New York, NY, USA, 2008.

23. Franklin, J.; Phinn, S.; Woodcock, C.; Rogan, J. Rationale and conceptual framework for classification approaches to assess forest resources and properties. *Remote Sensing of Forest Environments: Concepts and Case Studies*, Wulder, M., Franklin, S., Eds.; Kluwer Academic Publishers: Boston, MA, USA, 2003; pp. 279–300.

24. Rouse, J.; Hass, R.H.; Schell, J.A.; Deering, D.W. Monitoring vegetation systems in the Great Plains with ERTS. In *Third Earth Resources Technology Satellite-1 Symposium,* Greenbelt, MD, USA, *NASA SP-351*, 1974; pp. 3010–3317.

25. Landis, J.; Koch, G. The measurement of observer agreement for categorical data. *Biometrics* **1977**, *33*, 159–174.